frontiers | Frontiers in Environmental Science

TYPE Original Research
PUBLISHED 13 October 2023
DOI 10.3389/fenvs.2023.1252926

OPEN ACCESS

EDITED BY
Vishal Tripathi,
Graphic Era University, India

REVIEWED BY
Titus Egbosiuba,
Chukwuemeka Odumegwu Ojukwu University, Nigeria
Naveen Bunekar,
Chung Yuan Christian University, Taiwan

*CORRESPONDENCE
Mariem Zouari,
mariem.zouari@innorenew.eu

RECEIVED 04 July 2023
ACCEPTED 02 October 2023
PUBLISHED 13 October 2023

CITATION
Zouari M, Marrot L and DeVallance DB (2023), Evaluation of properties and formaldehyde removal efficiency of biocarbon prepared at variable pyrolytic temperatures.
Front. Environ. Sci. 11:1252926.
doi: 10.3389/fenvs.2023.1252926

Evaluation of properties and formaldehyde removal efficiency of biocarbon prepared at variable pyrolytic temperatures

Mariem Zouari[1,2]*, Laetitia Marrot[3] and David Brian DeVallance[4]

[1]InnoRenew CoE, Izola, Slovenia, [2]Faculty of Mathematics, Natural Sciences, and Information Technologies, University of Primorska, Koper, Slovenia, [3]Fire Safe Sustainable Built Environment (FRISSBE), Slovenian National Building and Civil Engineering Institute (ZAG), Ljubljana, Slovenia, [4]College of Science and Technology, Commonwealth University, Lock Haven, PA, United States

Biocarbon (BC) represents a potential material for application in air remediation. This study investigated the efficiency of BC particles in the removal of formaldehyde. BC samples were prepared from *Arundo donax* (AD) and olive stone (OS) feedstocks at variable pyrolysis temperatures (from 300°C to 800°C). The BC particles were characterized using proximate, Fourier transform infrared, water contact angle, particle size, and physisorption analyses. The formaldehyde removal capacity was tested using an electrochemical formaldehyde sensor in a batch experiment. The physicochemical and structural properties depended on the pyrolysis temperature at which the BC was produced. The increase in pyrolysis temperature increased the BC's pH, hydrophobicity, and porosity. All the samples achieved a formaldehyde removal capacity ranging between 26% and 64% for BC pyrolyzed at 300°C and 800°C, respectively. In BC pyrolyzed at temperatures under 500°C, the formaldehyde capture was governed by a partitioning mechanism through diffusion in the noncarbonized organic fraction. In comparison, formaldehyde capture was controlled by a physical adsorption mechanism through pore filling for BC pyrolyzed at 500°C or above. BC pyrolyzed at 800°C was more efficient for formaldehyde adsorption due to the well-developed microporous structure for both AD and OS. AD-derived BC prepared at 800 °C (AD-BC800) was selected for the re-usability test, using thermal regeneration to remove the adsorbed components. The regenerated sample maintained a comparable formaldehyde removal capacity up to four re-use cycles. Moreover, the comparison between non-activated and activated AD-BC800 revealed that physical activation significantly enhanced BC's adsorptive ability.

KEYWORDS

biocarbon, pyrolysis temperature, partitioning, adsorption, volatile organic compounds, air purification

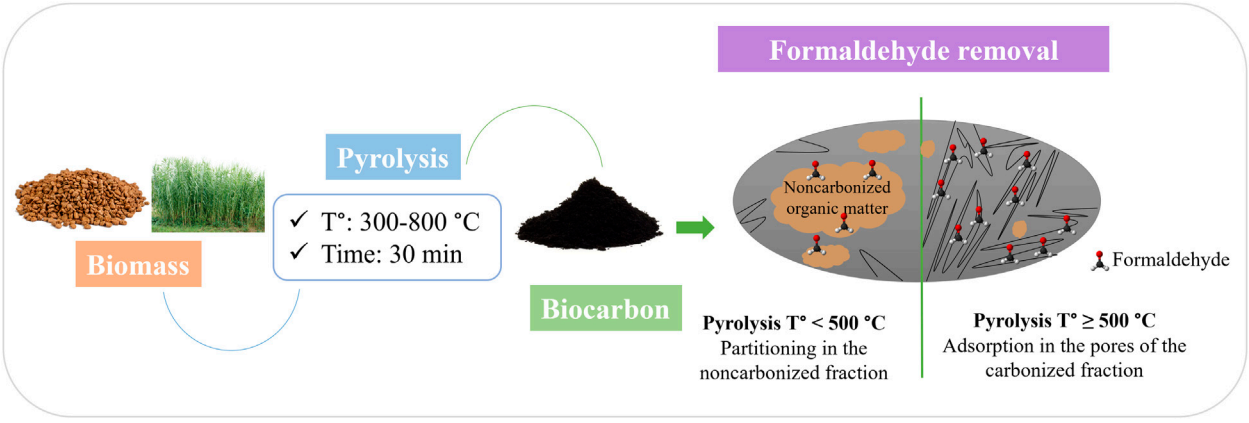

GRAPHICAL ABSTRACT

1 Introduction

Poor air quality is a severe problem linked to public health and environmental concerns. The World Health Organization reported in 2022 that air pollution is associated with 6.7 million premature deaths annually worldwide, from which 3.2 million deaths are caused by indoor air pollution (WHO, 2022). Among the wide range of airborne pollutants, volatile organic compounds (VOCs) have attracted more attention, given their high toxicity and negative environmental impact. VOCs are organic chemicals with high vapor pressure under ambient conditions, allowing them to evaporate and occur in the atmosphere. Depending on the boiling point range, VOCs can be categorized as very VOCs (from <0°C to 50°C–100°C), VOCs (from 50°C–100°C to 240°C–260°C), and semi-VOCs (from 240°C–260°C to 380°C–400°C) (WHO, 1989). VOCs represent a real threat to human health, given their high hazard and potential to provoke chronic severe diseases. Besides directly harming human health, VOCs damage the environment through photochemical smog formation and depletion of the ozone layer (Ling et al., 2019). Formaldehyde is an example of a common indoor VOC with a low evaporation point of about −19°C (IARC, 2006). In indoor conditions, formaldehyde is a colorless gas with an irritating odor and high reactivity. A large spectrum of indoor sources, such as flooring materials, carpets, cooking stoves, paints, and wall coverings, can emit formaldehyde. However, wood-based materials, such as furniture, are recognized as the primary emission source of formaldehyde in the indoor environment (Salthammer et al., 2010). Formaldehyde is a natural chemical in wood (Meyer and Boehme, 1997) primarily released during wood drying. Indoor emissions associated with wood product use are caused mainly by synthetic formaldehyde resin used as an adhesive component for commercial particle boards and furniture. Exposure to formaldehyde occurs by inhalation, and its consequences are various with several degrees of severity depending on concentration and exposure period: eye irritation, headache, dizziness, or acute symptoms such as respiratory tract damage, abortion, pneumonia, and hemorrhagic nephritis (US National Research Council, 1980). More serious concerns were raised after the classification of formaldehyde as a group 1 human carcinogen by the International Agency for Research on Cancer in 2006 (IARC, 2006).

Among the air remediation techniques, adsorption on porous support media has been recognized as a financially and technologically efficient method for trapping gaseous pollutants under ambient conditions. Carbonaceous materials such as carbon nanotubes (CNTs) (Liu et al., 2021), graphene (Guo et al., 2016), and activated carbon (Ryu et al., 2002) have been widely applied for the adsorption of a wide range of airborne pollutants. Biocarbon (BC), a member of the carbonaceous materials group, is a carbon-rich residue that can be prepared from the pyrolysis of almost any organic biomass, including underutilized feedstocks and by-products (Basu, 2013). BC, with and without activation, has been studied extensively as an adsorbent in soil or aqueous media for the removal of dye chemicals (Yu et al., 2021), heavy metals (Sachdeva et al., 2023), and antibiotics (Stylianou et al., 2021). BC has been shown to provide good adsorption performances in these applications due to its large porosity and surface functional groups. For instance, prior research (Egbosiuba et al., 2020) reported that activated BC from empty fruit bunch was successfully used for the removal of methylene blue from water. Results stated that the ultrasonic-assisted activation process enhanced the adsorption efficiency by increasing the porosity and surface chemistry of the adsorbent material. However, using BC for airborne contaminants removal has been less explored. BC's potential as an adsorbent is highly dependent on properties like porosity and carbon content (Angın, 2013). Pyrolysis temperature is the main factor determining the BC product's final properties and molecular structure (Leng and Huang, 2018). A prior study on the dynamic molecular structure of plant-derived BC (Keiluweit et al., 2010) revealed that depending on the pyrolysis temperature, BC could be categorized into four groups with differences in the chemical phases and physical states: 1) transition BC (from 200 °C to 300 °C with the release of light volatiles and evaporation of water, the crystalline structure of biomass is preserved), 2) amorphous BC (from 300°C to 600°C with depolymerization of the biomass and occurrence of random aromatic structures), 3) composite BC (from 600°C to 700°C with the generation of slightly ordered graphene-like arrangements merged into amorphous phases, and 4) turbostratic BC (above

700°C with the dominance of disordered graphitic crystallites). All these molecular and structural variations can influence the functionality of BC when used as an adsorbent (Keiluweit et al., 2010).

The efficiency of adsorbate-adsorbent interaction and the adsorption capacity can vary depending on the carbon material's properties. Thus, understanding the adsorption mechanism is crucial for preparing adequate material and achieving optimal pollutant removal. Yang et al. (2018) studied the kinetics of airborne pollutants adsorption on activated carbon with variable pores structures, and they concluded that the adsorption process occurs in three different phases. The first phase is external surface adsorption, when the adsorbate is transferred by convection and diffusion from the air to the adsorbent's surface. The rate of mass transfer depends on the specific surface area. The second phase is internal diffusion when the adsorbate molecules access the internal surface of the pores. The dominant factors in this phase are the pore size and volume. The final phase is the equilibrium stage, when the pores are filled with the adsorbate molecules. This stage depends on the ratio of different pore types (i.e., micro, meso, and macropores). Based on the above description of the adsorption mechanism, the adsorption capacity of porous materials, such as carbonaceous materials, was often associated with their physical structure. Notably, the specific surface area (SSA), pores size, and pores volume were believed to be key parameters controlling adsorption efficiency (Yang et al., 2018). For instance, Abdul Manap et al. (2018) studied formaldehyde adsorption on palm mesocarp-BC in a batch experiment. They reported that the formaldehyde adsorption increased with the increase of SSA and pores volume. However, their study did not investigate the microporous surface area, which could give complementary information to evaluate the relationship between adsorption capacity and the type of porosity.

Although the SSA and pores volume play an important role in the adsorption process, their effect in formaldehyde removal was not always dominant. Indeed, other factors could also contribute to formaldehyde adsorption on carbon-based materials, such as the basicity and the presence of surface functional groups. For instance, Lee et al. (2011) utilized sludge-derived activated carbon to remove formaldehyde. They reported that the sample activated with both KOH and ammonia performed better than the commercial activated carbon in removing formaldehyde despite the larger SSA of the commercial sample. They attributed the results to their prepared sample's higher surface basicity and content of oxygen and nitrogen functional groups. Based on their results, the surface basicity was favored by the occurrence of high amounts of metal components in the sewage sludge BC. However, this feature might not be representative of BC derived from other types of biomasses, such as AD and OS. Carter et al. (2011) also stated that the adsorption of low formaldehyde concentrations (3 and 7 ppm) was favored mainly by the presence of basic functional groups at the surface of activated carbon fibers (ACFs). Likewise, Yang et al. (2017) reported that CNTs-ACFs material exhibited three folds higher formaldehyde removal capacities than pure ACFs despite the significant difference in SSA (203.47 m^2/g and 1583.68 m^2/g for CNTs-ACFs and pure ACFs, respectively). They concluded that SSA could not accurately represent formaldehyde adsorption capacity. They also explained that the removal of formaldehyde, as a polar molecule, was likely enabled by chemisorption reactions that involve interaction and formation of strong covalent bonds between formaldehyde and the CNTs-ACFs material. The microporous surface area, pores distribution (i.e., micro, meso, and macropores), and composition of functional surface groups were not provided in their study which could further explain why CNTs-ACFs material performed better. The surface hydrophobicity of carbonaceous materials can also influence their adsorption capacity. In this regard, Boonamnuayvitaya et al. (2005) reported that the hydrophobic character of activated carbon samples lowered their ability to adsorb formaldehyde. They explained that formaldehyde, as a polar molecule, could better be adsorbed on hydrophilic surfaces. Based on their study, the formaldehyde adsorption capacity of activated carbon was more dependent on the surface chemical properties rather than the structural properties (i.e., surface area and pores volume).

During the present study, an in-depth investigation was performed to establish a better understanding of using BC as an efficient material for improving indoor air quality. The main objectives are: i) to investigate the effect of the pyrolysis temperature and physical activation on the properties of *Arundo donax* (AD) and olive stone (OS)-derived BC; ii) to investigate the influence of BC's properties on its formaldehyde removal capacity; and iii) to assess the re-usability of spent BC after thermal regeneration.

2 Materials and methods

2.1 Materials and reagents

Arundo donax (AD), an invasive species, and olive stone (OS), a by-product of the olive oil extraction industry, were selected as feedstocks. AD canes were harvested locally in Kampel, Slovenia. Crushed OS was provided by the Oljarna Krozera Franka Marzi sp olive oil extraction company (Srgaši, Slovenia) as by-products in 5 mm-sized dry particles.

The chemical composition of AD, is 21.1%, 37.9%, 34.0% for lignin, cellulose, and hemicellulose, respectively (Suárez et al., 2021).

The chemical composition of OS is 32.10%, 26.9%, and 34.8% for lignin, cellulose, and hemicellulose, respectively (Ferreiro-Cabello et al., 2022).

Technical N_2 with a purity of 99.998% (Grade 4.8) was used for the biomass pyrolysis and proximate analysis. N_2 and CO_2 gases with a purity of 99.999% (Grade 5.0) were used for physisorption analysis. Aqueous formaldehyde solution (37% w/v) was purchased from Carlo Erba reagents (Dasti group, Val de Reuil, France).

2.2 Preparation of the biomass

AD and OS were manually cleaned, ground with a cutting mill grinder (Pulverisette 25/19, Fritsch, Idar-Oberstein, Germany) using a 1 mm mesh, and dried in an oven for 24 h at 105°C to remove excessive moisture. The AD was then subjected to a demineralization

treatment by water washing under stirring at 60°C for 1 h to reduce the ash content. The OS, however, was not treated as our previous research indicated that the demineralization effect was negligible for this type of biomass (Zouari et al., 2023). Details about the characterization of the two biomasses can be found in (Zouari et al., 2023).

2.3 Preparation of the biocarbon particles

BC was prepared by pyrolysis of the two biomasses in a tube furnace (Nabertherm RSRC 120-1000/13, Nabertherm, Lilienthal, Germany). Each biomass, AD and OS, was pyrolyzed separately for 30 min at variable temperatures (300, 400, 500, 600, 700, and 800°C) under N_2 gas flow of 300 L/h and a heating rate of 1500°C/h, which is automatically controlled by the tube furnace and optimized to fit in the configuration of slow pyrolysis and to be able to control the thermal inertia of the furnace.

The pyrolysis process generated 12 specimens which were labelled based on the type of original biomass (AD or OS) and the pyrolysis temperature: AD-BC300, AD-BC400, AD-BC500, AD-BC600, AD-BC700, AD-BC800, OS-BC300, OS-BC400, OS-BC500, OS-BC600, OS-BC700, OS-BC800.

After cooling to room temperature, the BC samples were weighed to determine the pyrolysis yield using Eq. 1.

$$\text{Pyrolysis yield} = \frac{W_f}{W_i} \times 100 \quad (1)$$

Where W_i is the weight of the raw biomass (g), and W_f is to the weight of the derived BC (g).

The collected BC powders were then ball milled in distilled water media using a planetary ball miller (Pulverisette 5, Fritsch, Idar-Oberstein, Germany) for 30 min at 400 rpm. For milling, stainless-steel jars and 20 mm in diameter balls were utilized, and the ball: BC ratio was equal to 100. The ball-milled specimens were then dried at 105°C for 24 h to allow water evaporation, and the obtained powders were stored in glass containers until further characterization. The AD-BC800 sample was also processed through an activation phase to compare formaldehyde removal between non-activated and activated BC. AD-BC800 was selected for activation based on the formaldehyde removal results and a specific interest in valorizing AD as an invasive species. The BC activation was performed via physical activation under a CO_2 gas flow of 300 L/h at 800°C for 1 h. The obtained sample was identified as: Activated AD-BC800.

2.4 Characterization of the biocarbon particles

Proximate analysis was performed using a thermogravimetric analyzer (LECO TGA801, LECO corporation, Saint-Joseph, MI, United States). The volatiles, ash, and fixed carbon contents were determined according to the ASTM D7582 standard. Values for moisture, volatiles, ash, and fixed carbon were calculated using Eqs 2–5 detailed as specified in Section 14 of ASTM D7582 (ASTM, 2015).

$$\text{Moisture} = \frac{W_{initial} - W_{107°C}}{W_{initial}} \times 100 \quad (2)$$

$$\text{Volatiles} = \frac{W_{107°C} - W_{950°C}}{W_{initial}} \times 100 \quad (3)$$

$$\text{Ash} = \frac{W_{750°C}}{W_{initial}} \times 100 \quad (4)$$

$$\text{Fixed carbon} = 100 - (Moisture + Volatiles + Ash) \quad (5)$$

Where $W_{initial}$ is the initial weight of the BC sample (g), and $W_{*°C}$ refers to the weight of the BC sample (g) at the designated * temperature.

All tests were repeated three times, and the average values were reported.

The pH was measured in the leachate of the BC specimen by first mixing 0.5 g of BC with 10 mL of deionized water and agitating the mixture in an incubation shaker (IS-OS 20, Phoenix Instruments, Naperville, Illinois, United States) at 23 °C for 1 h. The solutions were then left to settle for 30 min, and the pH was determined using a pH meter equipped with an IS-68 × 591206-B-VSTAR pH/LogR Module (Orion Versa-Star Pro Meter, Thermo Fischer Scientific, Waltham, Massachusetts, United States).

Functional groups on the BC surface were analyzed using a Fourier transform infrared (FTIR) spectrometer (Alpha FT-IR Spectrometer Bruker, Billerica, MA, United States) connected to an ATR (attenuated total reflection) module. Wavelength ranges from 400 to 4,000 cm^{-1}, and a resolution of 4 cm^{-1} was set to record the FTIR spectra. For each sample, 64 scans were performed, and ten repetitions were done to obtain accurate results and minimize the effect of the atmospheric noise. Opus software was used to collect average spectra, which were further treated by eliminating CO_2 and atmospheric water vapor effects.

Hydrophobicity was assessed by an optical tensiometer (Attension Theta Flex Auto 4 system, Biolin Scientific, Gothenburg, Sweden) that measured the dynamic water contact angle (WCA). Following the method reported by Bachmann et al. (2000), the BC powders were evenly spread and pressed as a thin layer on a flat glass surface covered with adhesive tape (with the adhesive side exposed to the BC particles for proper fixation). The sessile drop method was used to determine the WCA. Five droplets, 4 μL each, were placed on the BC powders, and the WCA value was taken at 30 s. Averages with standard deviations were reported.

The particle size distribution was determined by laser diffraction technique using a Horiba Scientific LA-960A2 analyzer (HORIBA, Kyoto, Japan). The refractive index was set to 1.92. Before each measurement, 1 min of ultrasonication was done to facilitate homogeneous dispersion of the particles. Three repetitions were performed for each sample, and the average values were reported.

The internal porosity of the BC particles was investigated using a physisorption analyzer (Anton Paar Quantachrome Instruments, Boynton Beach, Florida, United States). N_2 and CO_2 gases were used to evaluate the surface area and pores distribution according to Brunauer-Emmett-Teller (BET) and Barrett, Joyner, and Halenda (BJH), and density functional theory (DFT) models, respectively. Before analysis, samples were degassed under vacuum for 12 h at 250°C to remove impurities trapped in the BC's cavities. Then, for the BET model, the N_2 adsorption-desorption isotherms were determined over a relative pressure range from 0.005 bar to 1 bar

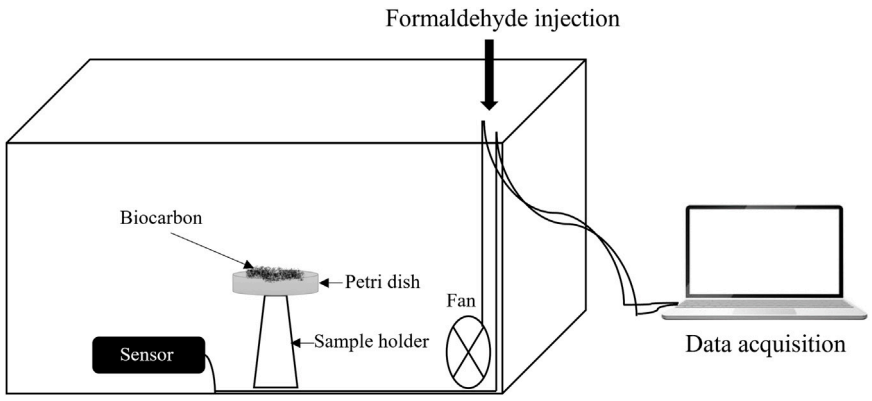

FIGURE 1
Schematic illustration of the formaldehyde removal capacity testing setup.

TABLE 1 Composition and pH of the biocarbon particles.

Sample ID	Proximate composition, % (mass-based)			pH	Pyrolysis yield, %
	Volatiles	Ash	Fixed carbon		
AD-BC300	58.21 ± 1.03	6.88 ± 0.14	31.81 ± 1.23	4.27 ± 0.05	53
AD-BC400	30.09 ± 0.60	6.29 ± 0.30	59.78 ± 0.79	4.28 ± 0.01	30
AD-BC500	20.96 ± 0.47	8.89 ± 0.28	65.43 ± 0.71	6.47 ± 0.05	27
AD-BC600	13.87 ± 0.30	7.24 ± 0.16	74.83 ± 0.46	8.43 ± 0.02	24
AD-BC700	12.65 ± 0.55	8.93 ± 0.10	76.02 ± 0.32	8.50 ± 0.06	23
AD-BC800	10.80 ± 0.52	10.75 ± 0.11	76.21 ± 0.59	8.63 ± 0.05	23
Activated AD-BC800	12.22 ± 0.39	13.11 ± 0.19	71.92 ± 0.66	8.92 ± 0.02	23
OS-BC300	49.36 ± 1.01	2.03 ± 0.04	46.87 ± 0.96	5.23 ± 0.01	53
OS-BC400	31.60 ± 0.70	2.47 ± 0.16	62.05 ± 0.94	5.69 ± 0.03	35
OS-BC500	22.21 ± 0.35	3.01 ± 0.03	73.24 ± 0.72	7.18 ± 0.04	33
OS-BC600	14.4 ± 0.41	2.29 ± 0.02	81.04 ± 0.73	8.33 ± 0.08	27
OS-BC700	11.45 ± 0.83	1.93 ± 0.58	83.78 ± 0.40	8.01 ± 0.07	27
OS-BC800	9.92 ± 0.60	4.29 ± 0.27	83.89 ± 0.87	8.71 ± 0.07	25

at 77 K to determine SSA and total pores volume, represented by mesopores (2 nm–50 nm in width) and macropores (>50 nm in width). In addition, the BJH method was used to determine the meso and macropores size distribution. For the DFT model, CO_2 adsorption-desorption isotherms were collected at a pressure range from 0.001 bar to 0.03 bar at 273 K to determine microporous surface area and micropores (<2 nm in width) volume.

2.5 Formaldehyde removal efficiency tests

The formaldehyde removal performance of the different BC samples was evaluated using a batch experiment setup, as shown in Figure 1. Before the tests, the samples were oven-dried overnight at 105 °C to remove any residual moisture. Tests were carried out in a closed glass chamber with a volume of 54 L equipped with an electrical fan. A Petri dish containing 1 g of BC powder sample was placed inside the testing chamber on a glass support, and 35 µL of formaldehyde solution was injected into the chamber through the inlet using a 50 µL micropipette. The chamber was hermetically sealed, and the fan was turned on to ensure a homogeneous distribution of the formaldehyde molecules. The initial formaldehyde concentration stabilized at 4 ppm. The experiment was conducted in standard ambient conditions: 23°C temperature, 50% relative humidity, and atmospheric pressure. The changes in formaldehyde concentration inside the chamber were continuously recorded using a formaldehyde electrochemical detection sensor (Stox-HCHO, EC Sense, Schäftlarn, Germany) with 0.1 ppm resolution and 1 s response time. The sensor was connected to the computer,

which enabled direct data acquisition using a TVOC-HCHO logger software (ADDproS, Celje, Slovenia).

The formaldehyde removal percentages were calculated according to Eq. 6 (Do et al., 2022), using the residual pollutant concentration measured in the chamber after 1 h.

$$\text{Formaldehyde removal} = \frac{C_0 - C_{1h}}{C_0} \times 100 \quad (6)$$

Where C_0 is the initial formaldehyde concentration (ppm) and C_{1h} is the measured formaldehyde concentration after 1 h of the experiment (ppm).

A blank test was carried out by repeating the same experiment without BC particles. The reduction in pollutant concentration calculated for the blank was subtracted from the values obtained for each sample for results correction. Three repetitions were conducted per BC substrate, and the average values were reported.

The re-usability of the spent adsorbent, AD-BC800, was assessed by determining the formaldehyde removal capacity after five cycles of thermal regeneration. The BC specimen was placed in the oven at 100 °C for 1 h to desorb the formaldehyde molecules captured in the BC pores during the previous cycle.

2.6 Statistical analysis

The Pearson correlation test was used to evaluate the relationship between BC's properties and the formaldehyde removal capacity. Furthermore, the effect of BC's properties on the formaldehyde removal capacity was evaluated by performing a multiple regression analysis. For both analyses, variables from all samples (AD-BC and OS-BC) were evaluated to remove the biomass type effect. NCSS software (NCSS, LLC, Version 07.1.21) was used for the statistical analysis. The effect of the independent variable was considered to be significant when the *p*-value was below 0.05.

The formaldehyde removal capacity of AD-BC and OS-BC was compared by unpaired *t*-test in Excel. A paired *t*-test was performed to compare the formaldehyde removal performance of non-activated and activated BC.

3 Results and discussion

3.1 Characteristics of biocarbon particles

3.1.1 Composition and pH

Results from proximate analysis, pH measurements, and pyrolysis yield of the BC samples derived from AD and OS at different pyrolytic temperatures are shown in Table 1.

The yield in BC decreased with the increase of the pyrolysis temperature from 300°C to 800°C. As the temperature increased from 300 °C to 500 °C, a decrease in the yield was observed from 53% to 27% for AD and from 53% to 33% for OS. However, when the temperature went from 600°C to 800°C, the yield slowly decreased from 24% to 23% for AD and 27%–25% for OS. The main lignocellulosic mass degradation occurred from 300°C to 500°C, resulting in a high amount of volatiles being released. Indeed, prior research (Marrot et al., 2021) on hemp stem pyrolysis reported that the maximum biomass degradation associated with maximum mass loss occurred at temperatures between 335 °C and 406 °C (for thermograms obtained with a heating rate of 2000 °C/h). Regardless of the pyrolysis temperature, OS yielded more BC compared to AD (Table 1), which can be assigned to the higher lignin content in OS of 26.50% (Rodríguez et al., 2008) *versus* 21.11% in AD (Suárez et al., 2021). Lignin-rich biomasses tend to generate more BC given the high thermal resistance and slow degradation of lignin polymers, starting at ambient temperature and continuing up to 900°C (Yang et al., 2007). This explanation aligns with the proximate analysis results (Table 1), revealing OS-derived BC samples' higher fixed carbon content.

When the pyrolysis temperature increased from 300°C to 800°C, the volatiles content decreased from 58.21% ± 1.03% to 10.80% ± 0.52% for AD-BC and from 49.36% ± 1.01% to 9.92% ± 0.60% for OS-BC samples. An opposite trend was obtained for ash and fixed carbon contents, which increased proportionally. As pyrolysis temperature increased, more volatile matter generated by the decomposition of biomass components was released in the form of condensable and non-condensable gases, promoting carbon-rich residue and concentration of ash minerals. Similar findings were reported by Marrot et al. (2021), who reported a decrease in volatiles and an increase in ash and fixed carbon percentages when the temperature increased from 400 °C to 1000 °C when preparing hemp stem-based BC. Egbosiuba (2022) also reported that the fixed carbon content of cassava peel-derived BC increased gradually with the increase in pyrolysis temperature from 300 °C to 600 °C regardless of the applied heating rate (10, 20, or 30 °C/min).

Regarding BC pH, the pH measurements increased progressively. They changed from an acidic character for samples prepared at 300 °C (4.27 ± 0.05 and 5.23 ± 0.01 for AD and OS, respectively) to an alkaline character for samples prepared at 800 °C (8.63 ± 0.05 and 8.71 ± 0.07 for AD and OS, respectively). Above 500°C, pH values fluctuated slightly for both biomasses, while it fluctuated clearly between samples prepared under 500°C. The lower pH observed for BC pyrolyzed at temperatures under 500 °C is likely related to higher amounts of acidic carboxyl groups in hemicellulose and celluloses, which were not degraded at these lower temperatures. Another reason for the increase in pH values could be the accumulation of ash components that have an alkaline nature. A prior study (Van Krevelen, 1993) assigned the decrease in BC's acidity at high temperatures to convert acidic aliphatic groups in the organic material into alkaline aromatic groups.

3.1.2 Surface functional groups of raw biomasses and their derived biocarbon particles

Figure 2 represents the FTIR spectra for raw biomasses, and the resultant BC produced at different pyrolysis temperatures. The detected peaks corresponding to surface functional groups were highlighted, and it can be observed that spectra from both biomasses revealed the presence of peaks in similar positions. Moreover, functional groups were more diverse in BC samples prepared at lower temperatures (<500 °C) regardless of the biomass type.

With the increase of pyrolysis temperature, a decrease in the polar O-H stretching (3,200–3,500 cm^{-1}) correspondent to hydroxyl groups was observed, which was attributed to the dehydration reactions due to water evaporation besides the degradation of alcohols and carboxylic groups (Keiluweit et al., 2010). The

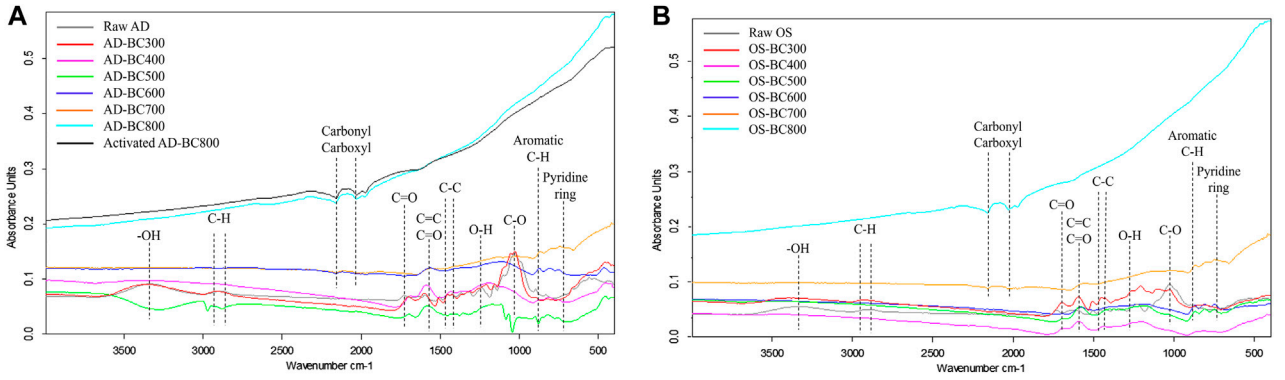

FIGURE 2
FTIR spectra of the raw biomasses and their derived biocarbon particles: **(A)** *Arundo donax* and **(B)** olive stone.

degradation of carboxylic groups correlated well with the reduction in BC's acidity (increase in pH) at higher temperatures (Table 1).

The peak at 2,925 cm^{-1} assigned to asymmetrical and symmetric-CH vibrations was detected in raw biomasses, and BC prepared at 300 °C. Then this peak faded to vanish in the rest of the BC samples. The -CH vibrations disappeared with the increase in pyrolysis temperature due to the decomposition of cellulose and hemicellulose, usually occurring at a temperature range of 220°C–400°C (Yang et al., 2007).

The band at 1750 cm^{-1} assigned to C=O functional groups from esters and anhydrides was present in the raw and carbonized biomasses at 300°C. The same band was also observed with lower intensity in BC samples prepared at 400°C. Then, this band disappeared as the pyrolysis temperature further increased.

The band at 1600 cm^{-1} associated with aromatic C=C and C=O stretching of alkenes and aldehydes, respectively (Uchimiya et al., 2011), was slightly present in the raw biomass spectra. This band then increased gradually with the increase in pyrolysis temperature up to 600°C, which positively correlates with the results from proximate analysis (Table 1) that revealed an increase in the fixed carbon content. However, the same band was not present in spectra corresponding to samples prepared at 700 °C and 800°C, likely because of high enough energy (high temperature), which enabled the breakage of these groups. Stretching around 890 cm^{-1} correspondent to C-H aromatic rings (Sahoo et al., 2020) was detected in all BC samples except for those prepared at 700°C and 800°C. During pyrolysis from 300°C to 600°C, the aromaticity of BC increased as the thermolabile aliphatic groups in raw biomass transformed into more stable aromatic structures. However, a further increase in the temperature (i.e., above 600°C) likely destroyed these structures. Similarly, Sahoo et al. (2020) observed an increase in C-H aromatic rings in BC from 350°C to 550°C, which was attributed to the simultaneous decrease in OH and CH alkyl groups. At 650 °C, they recorded a decrease in the peak of C-H aromatic rings, which was explained by the breakage of aromatics to generate more volatile compounds.

The wide band between 2050 cm^{-1} and 2,200 cm^{-1} was ascribed to carboxyl and carbonyl groups (Angin, 2013). This band was absent in BC prepared at 300°C–600°C, appeared slightly at 700°C and was visible at 800°C. The occurrence of this band is associated with the formation of different carbon structures (aromatic, carboxylic, and carbonyl carbon) at high pyrolytic temperatures. A prior study (Marrot et al., 2023) reported a similar trend in hemp BC samples pyrolyzed at 400°C–1000°C.

TABLE 2 Hydrophobicity test results.

Pyrolysis temperature, °C	Water contact angle, °	
	AD- BC	OS-BC
300	105 ± 13	97 ± 7
400	107 ± 5	125 ± 1
500	116 ± 4	126 ± 2
600	122 ± 1	130 ± 2
700	127 ± 1	131 ± 2
800	128 ± 1	141 ± 6
800 and CO_2 activation	128 ± 2	—

The stretching observed at 1400 cm^{-1} correspondent to C-C rings in lignin (Nandiyanto et al., 2016) was detected in raw biomasses, and BC prepared at 300°C and 400°C. As the pyrolysis temperature increased above 400°C, lignin polymers gradually degraded, leading to less pronounced peaks of C-C rings.

The FTIR spectra also revealed that the band at 1050 cm^{-1}, associated with C-O symmetric stretching for aliphatic functional groups, was soundly prominent in raw AD and OS. However, this band was detected with lower intensity in the BC sample prepared at 300°C and disappeared in BC prepared at temperatures above 300°C. This result was attributed to the depolymerization and degradation of celluloses and hemicelluloses during pyrolysis at high temperatures.

The activated AD-BC800 sample had an FTIR spectrum similar to the non-activated sample. Thus, the physical activation treatment did not influence the functional group composition at the surface of the BC sample in this case.

FTIR analysis results suggested that the pyrolytic temperature influenced the functional group composition of BC samples regardless of the raw biomass type. The change in functional

TABLE 3 Particle size representative diameters of the biocarbon samples.

Sample ID	Cumulative particle size distribution			
	D_{10}, μm	D_{50}, μm	D_{90}, μm	Mean, μm
AD-BC400	9 ± 4	20 ± 3	358 ± 11	88 ± 5
AD-BC500	5 ± 2	17 ± 2	270 ± 9	62 ± 4
AD-BC600	6 ± 1	15 ± 1	67 ± 5	31 ± 2
AD-BC700	5 ± 1	12 ± 2	37 ± 2	20 ± 2
AD-BC800	4 ± 2	11 ± 1	20 ± 3	16 ± 2
Activated AD-BC800	3 ± 1	11 ± 2	25 ± 1	13 ± 1
OS-BC300	6 ± 3	21 ± 3	101 ± 6	31 ± 3
OS-BC400	3 ± 1	12 ± 3	87 ± 4	31 ± 2
OS-BC500	2 ± 2	10 ± 2	64 ± 5	28 ± 3
OS-BC600	2 ± 1	7 ± 1	16 ± 3	9 ± 2
OS-BC700	2 ± 2	8 ± 2	17 ± 1	9 ± 2
OS-BC800	1 ± 1	6 ± 1	15 ± 2	7 ± 2

groups resulted from the biomass degradation reactions during the pyrolysis process.

3.1.3 Hydrophobicity of the biocarbon particles

The mean values of the water contact angle (WCA) of the BC powders are listed in Table 2.

Regardless of the original biomass type and pyrolysis temperature, all BC specimens exhibited a hydrophobic character (i.e., WCA higher than 90° (Law, 2014), and the higher the WCA, the stronger the water repellency). The WCA constantly increased with an increase in the pyrolysis temperature from 300 °C to 800 °C for both BC derived from AD and OS. Results were attributed to the changes in the chemical composition of the material prepared at different temperatures. With the increase in pyrolysis temperature, the extent of thermal degradation increased, and less hydrophilic natural polymers, namely cellulose and hemicellulose, were present in the final BC materials. Therefore, the BC prepared at higher temperatures exhibited higher hydrophobicity.

For BC prepared at 300°C, the WCA was higher (105° ± 13°) in the case of the AD-derived sample as compared to the OS-derived sample (97 ± 7). However, for BC prepared at temperatures from 400 °C to 800°C, the AD-derived samples had a lower WCA than the OS-derived samples (Table 2). These findings are likely related to the original chemical composition (i.e., the ratio of hemicellulose, cellulose, and lignin) of the two different feedstocks, which could affect the nature and intensity of the functional groups in the derived BC samples. The lower hydrophobicity of AD-derived BC was likely attributed to AD having a higher hemicellulose and cellulose content than OS. Suárez et al. (2021) reported a hemicellulose and cellulose content in AD of 34.02% and 37.95%, respectively, while Ferreiro-Cabello et al. (2022) reported a hemicellulose and cellulose content in OS of 34.8% and 26.9%, respectively.

The WCA of AD-BC800 remained steady after physical activation. Thus, the activation treatment did not affect the hydrophobicity of the material. The BC's hydrophobicity depended on the pyrolytic temperature and the original feedstock type. These results indicate that BC's hydrophobic properties can be tailored by selecting specific initial feedstock and processing temperatures.

3.1.4 Particles size of the biocarbon particles

Size distributions of the BC samples derived from AD and OS are represented in Table 3. Percentile values D_{10}, D_{50}, and D_{90} are statistical representatives for the cumulative particle size distribution where they indicate the size below which 10%, 50%, and 90% of all particles are obtained, respectively.

The ball-milling treatment of BC effectively reduced the particles' size as the particle size distributions of all samples fit into the micro-size range (Table 3). The AD-derived BC samples had a slightly higher particle size distribution than OS-derived BC. The mean size ranged between 13 μm and 88 μm and between 7 μm and 31 μm for BC derived from AD and OS, respectively. The difference in particle size between BC and different biomasses might be related to the shape of the raw biomass particles, round for OS and fibrous for AD (sheet-like particles). Indeed, the particle's shape can influence the particle size results when using laser diffraction, given that rod-shaped particles tend to appear larger (Naito et al., 1998).

Interestingly, the particle size decreased with the increase in pyrolysis temperature regardless of the biomass type. Exposure to higher temperatures provoked further degradation of the biomass components (i.e., hemicellulose, cellulose, and lignin), which likely decreased the resistance of the generated BC particles against the mechanical force during the ball-milling process. Thus, higher pyrolysis temperatures favored the grindability of BC.

3.1.5 Porosity of the biocarbon particles

The adsorption-desorption isotherms of N_2 and CO_2 in AD and OS-derived BC are represented in Figures 3, 4, respectively. Detailed results from the physisorption analysis are summarised in Table 4. The isotherms showed that BC samples prepared at variable temperatures possessed different N_2 and CO_2 uptake at a given relative pressure.

For N_2 adsorption-desorption isotherms, an open structure (i.e., separated adsorption-desorption branches) was observed, which is usually characteristic of carbon-based materials with narrow pores. For both biomasses, the N_2 isotherm of BC samples prepared at a temperature above 500 °C and the activated AD sample conformed with the type I isotherm characterized by strong N_2 uptake at low pressure according to the classification made by the International Union of Pure and Applied Chemistry (IUPAC) (Thommes et al., 2015). The sharp increase in the N_2 uptake close to the saturation vapor pressure (i.e., 1) is attributed to large meso- and macro-pores filling. The Activation of AD-BC800 further enhanced the N_2 uptake (Figure 3A), suggesting that physical activation further expanded the porosity of the BC sample.

The CO_2 adsorption-desorption isotherms had closed adsorption-desorption branches, and no hysteresis was observed, indicating that CO_2 molecules could be completely and easily desorbed. The capacity of CO_2 uptake increased gradually with

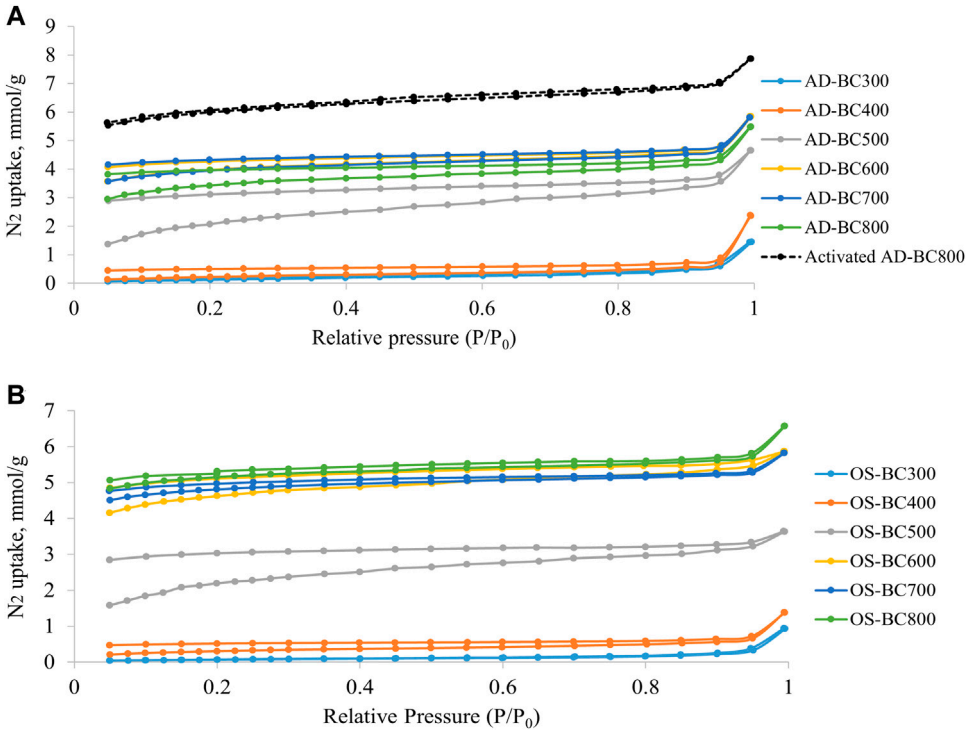

FIGURE 3
N_2 adsorption–desorption isotherms obtained at 77 K for **(A)** *Arundo donax* and **(B)** olive stone-derived biocarbon prepared at different pyrolysis temperatures.

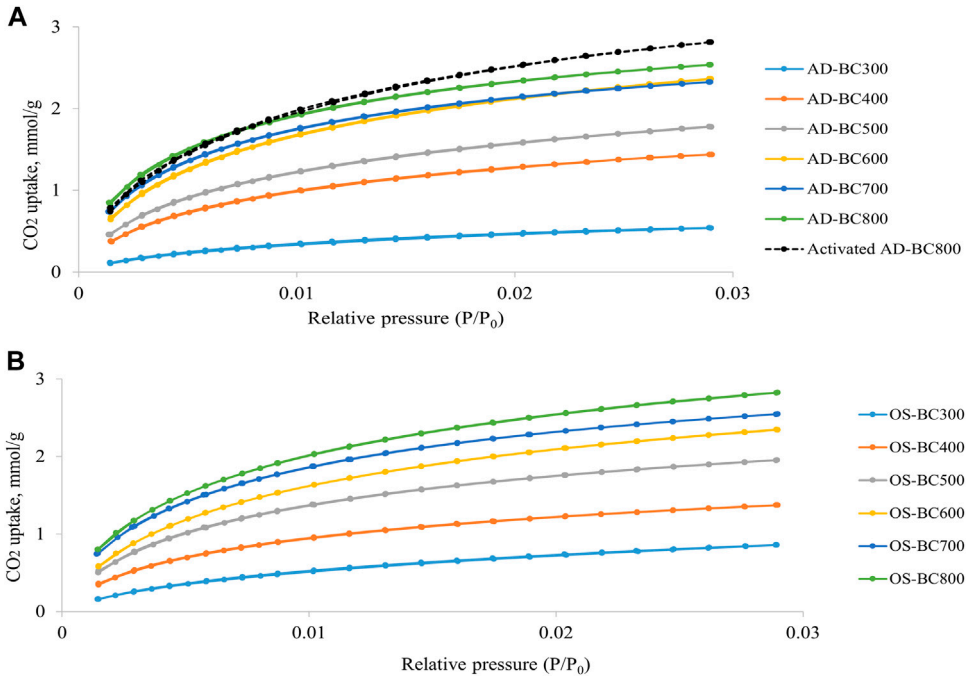

FIGURE 4
CO_2 adsorption–desorption isotherms obtained at 273 K for **(A)** *Arundo donax* and **(B)** olive stone-derived biocarbon prepared at different pyrolysis temperatures.

TABLE 4 Summary of physisorption analysis results.

Sample ID	Nitrogen		CO_2	
	Specific surface area, m^2/g	Total pore volume, cm^3/g	Microporous surface area, m^2/g	Micropores volume, cm^3/g
AD-BC300	13.82	0.050	125.27	0.038
AD-BC400	19.72	0.082	320.51	0.085
AD-BC500	177.15	0.162	414.50	0.116
AD-BC600	334.87	0.202	544.00	0.147
AD-BC700	332.80	0.203	540.20	0.140
AD-BC800	291.40	0.190	587.18	0.151
Activated AD-BC800	415.61	0.273	664.16	0.187
OS-BC300	6.01	0.032	208.96	0.067
OS-BC400	24.28	0.048	320.68	0.090
OS-BC500	167.44	0.126	450.57	0.123
OS-BC600	325.35	0.263	543.15	0.151
OS-BC700	330.94	0.202	589.38	0.156
OS-BC800	354.54	0.228	647.89	0.172

the increase of the relative pressure. The highest CO_2 uptakes were achieved by AD and OS BC prepared at 800°C, indicating that higher pyrolytic temperature favored the development of microporous structure in the BC samples. The Activated AD-BC800 exhibited higher CO_2 uptake as compared to the non-activated sample. Thus, physical activation treatment boosted the formation of micropores in the BC.

The specific and microporous surface areas and pore volumes of BC samples increased with the increase of pyrolysis temperature from 300°C to 800°C regardless of the original biomass type (Table 4). As pyrolysis temperature increased, the released volatiles generated cavities and pores in the BC structure. At higher pyrolysis temperatures, the extent of thermal degradation increased, and more volatiles were released, which was reflected by larger values of surface area and pores volume. A similar trend was observed by Mao et al. (2019), who found that the specific and micro porosities of the BC prepared from several types of feedstocks (pine wood, rice straw, rice bran, wood sawdust, and orange peels) were enhanced by increasing the pyrolysis temperature (250, 500, and 700 °C).

Except for the pyrolytic temperature of 300°C, AD-derived BC's SSA and microporous surface area were lower than those of OS-derived BC samples (Table 4). These results are likely related to the raw biomasses' original chemical composition, which might have influenced the thermal decomposition pathways during pyrolysis. Similarly, Lu and Zong. (2018) reported that the SSA of BC prepared from coniferous forest wastes was higher than that of BC prepared from herbaceous plant and broad-leaf forest wastes. They justified that the differences in porosity characteristics of BC from different feedstocks were related to the differences in cell morphology and structure in the raw materials. They also concluded that the precursor biomass types influenced BC's internal structure.

The increment in SSA was continuous in the function of the pyrolysis temperature for OS-derived BC samples. However, in the case of AD-derived BC, the SSA increased gradually up to 600 °C, then decreased slightly at 700°C and 800°C. These results can be seen in the N_2 adsorption-desorption isotherms (Figure 3A), where AD-BC600 had the highest N_2 uptake amongst other AD-BC. However, the microporous surface area of AD-BC800 was higher than AD-BC600, which was reflected in the CO_2 adsorption-desorption isotherms (Figure 4A). These findings suggest the effect of pyrolysis temperature on the BC's porosity could vary with the type of original biomass. Interestingly, regardless of the biomass type, BC's SSA increased sharply when the pyrolysis temperature went from 400°C to 500°C. This increase was attributed to the condensation of aromatics in lignin (happening around 500 C), which led to the generation and quick release of high amounts of gases and forced the opening of smaller pores). The total pore size distribution plots (Supplementary Figure S1) showed the dominance of mesopores with sizes ranging from 3 to 5 nm in all samples. However, these narrow mesopores occurred less in samples prepared under 500 C (Supplementary Figures S1A, B) than in samples pyrolyzed at 500 °C or above (Supplementary Figures S1C–F). Likewise, the micropore distribution (obtained from CO2 physisorption analysis) showed micropore sizes between 0.35 and 0.60 nm (Supplementary Figure S2). The structures of BC prepared at 500°C or above contained a larger volume of ultra-micropores. Therefore, the high pyrolytic temperatures favored biomass devolatilization and led to the resulting microporous structures in BC.

The activated AD-BC800 sample had larger surface areas and pore volume than the non-activated sample (Table 4). The SSA and

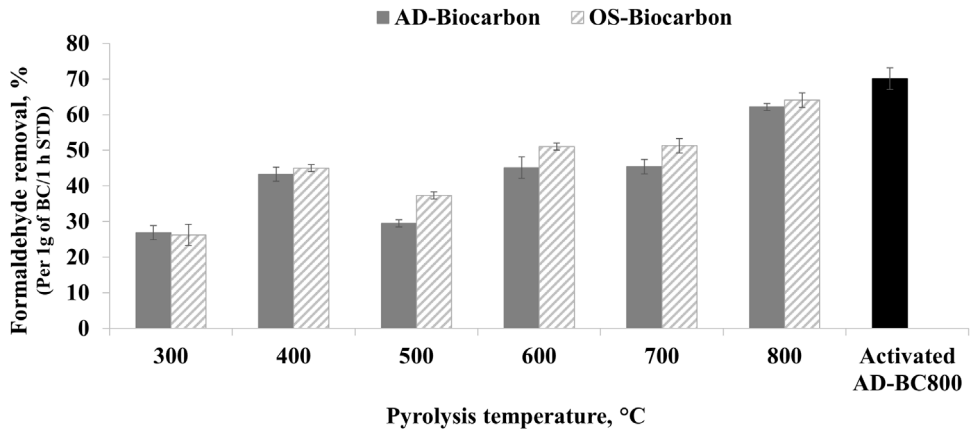

FIGURE 5
Formaldehyde removal capacities as a function of pyrolytic temperature.

TABLE 5 Correlation and multiple regression test results.

Independent variables	Correlation		Multiple regression
	Correlation coefficients	*p* Values	*p* Values
Fixed carbon, %	0.777	0.002*	0.421
Volatiles, %	−0.759	0.004*	0.250
Specific surface area, m^2/g	0.682	0.014*	0.054
Microporous surface area, m^2/g	0.815	0.001*	0.022*

* Statistically significant.

microporous surface area increased by 43% and 14% after activation. Therefore, the physical activation treatment further developed the BC's porosity.

3.2 Formaldehyde removal capacity

The formaldehyde removal percentages calculated after 1 h of experimental time in the presence of 1 g of BC are presented in Figure 5. The BC samples prepared at different temperatures exhibited different formaldehyde removal potentials. Indeed, the variation of pyrolytic temperature influenced the physicochemical and structural properties of the resulting BC samples and consequently changed the sorptive capacities. All BC samples achieved a certain formaldehyde removal activity. The percentage of formaldehyde removal ranged between 27% ± 2% and 62% ± 1% and between 26 ± 3%and 64% ± 2% for AD and OS-derived BC, respectively. Moreover, the amount of captured formaldehyde increased by 131% and 144% when the pyrolysis temperature increased from 300°C to 800 C for AD and OS-derived BC, respectively.

The correlation and multiple regression analysis results are represented in Table 5. The variables' effect was considered statistically significant when the corresponding *p*-value was below 0.05.

The correlation coefficients showed a positive correlation between formaldehyde removal capacity and fixed carbon, SSA, and microporous surface area. At the same time, a negative correlation was found between the formaldehyde removal capacity and the volatile content (Table 5). The *p* values from the correlation test showed a statistically significant relation between formaldehyde removal capacity and the four tested variables ($p < 0.05$). Results from the multiple regression analysis indicated that only microporous surface area was statistically significant when developing an equation to predict formaldehyde absorption based on BC properties. This result suggested that the occurrence of micropores in the BC's structure was the key parameter for efficient formaldehyde removal.

The unpaired *t*-test showed no statistically significant difference between the formaldehyde removal ability of BC prepared from AD and OS ($p = 0.311$). Therefore, the original feedstock did not influence the removal capacity. The slightly higher formaldehyde removal potential of OS-derived BC samples (Figure 5) was likely related to their larger microporous surface areas (Table 4) as compared to the AD-derived BC samples. Despite its lower SSA, AD-BC800 showed higher adsorption compared to AD-BC600. This result was attributed to the higher microporous surface area of AD-BC800 as compared to AD-BC600 (Table 4).

The presence of ultra-micropores concentrated in size range from 0.35 to 0.60 nm (Supplementary Figure S2) further confirms

the beneficial effect of smaller micropores occurrence on the BC's potential in removing formaldehyde. One possible explanation is the small size of the formaldehyde molecule, which has a diameter of 0.25 nm. The small size of the adsorbate was likely favorable for filling narrow micropores. Indeed, prior research reported that the adsorbate and pore size directly influence the adsorption capacity (Yang et al., 2018). Prior research (Yang et al., 2018) reported that the adsorption was not favored i) if the pore size of the porous material (i.e., adsorbent) is smaller than the target molecule's (i.e., adsorbate) size and ii) if the pore size is much larger than the molecule's size. Additionally, Liu et al. (2019) used molecular simulation models to investigate the kinetics of formaldehyde adsorption on carbonaceous materials and reported that ultra-micropores with 0.7 nm in width enabled optimal formaldehyde capture.

The increase in formaldehyde removal capacity by the different BC was not constant (Figure 5). Indeed, the formaldehyde removal increased when the temperature increased from 300°C to 400°C, then dropped at 500°C and increased again gradually from 600°C to 800°C. These results were attributed to two formaldehyde removal mechanisms and the predominance of one or the other. Indeed, Chen et al. (2008) highlighted that the pollutant removal by BC is ensured by either the partitioning effect and/or the adsorption effect. They also stated that the noncarbonized and carbonized fractions and surface and bulk properties of the BC material determine the contribution of either mechanism. In our study, the BC samples prepared at mild pyrolytic temperatures (under 500°C) had a higher noncarbonized organic matter content, reflected by the high volatiles and low fixed carbon content (Table 1). Noncarbonized organic matter likely favored the interaction with formaldehyde molecules and enabled the capture through a partitioning mechanism. During partitioning, the formaldehyde molecules diffused into the noncarbonized organic matter characterized by its amorphous aliphatic feature. This mechanism usually involves polar and non-polar interactions. Therefore, the presence of surface functional groups in BC samples prepared at 300°C and 400°C, observed in the FTIR spectra (Figure 2), likely helped to enable further the interaction forces between the formaldehyde molecules and the BC particles. Prior research by Meng et al. (2019) reported that functional groups on the surface of carbonaceous materials favored the interaction with gaseous VOCs.

For BC prepared at higher pyrolytic temperatures (500°C and above), the formaldehyde capture was assisted by the developed porous structure and large surface area. In this case, pores served as adsorption sites for the formaldehyde molecules and enabled the capture through a physical adsorption mechanism. Indeed, the adsorption phenomenon is mainly governed by Van der Waals forces, pores filling, and electrostatic adsorbent-adsorbate interaction (Vikrant et al., 2020). Therefore, the well-developed porosity, specifically microporosity, of the BC prepared at 500 °C and above (Table 4) was a key parameter in formaldehyde removal by BC, as verified by the multiple regression analysis (Table 5). Zhang et al. (2017) studied the performance of BC prepared from different biomasses at variable carbonization temperatures for air purification. They reported that the VOCs removal was governed by a partitioning mechanism in the case of BC prepared at 450°C or below and by a physical adsorption mechanism in the case of BC prepared at 600°C.

AD-BC800s formaldehyde removal capacity increased by 13% after physical activation (Figure 5). This increase was attributed to the improved microporous surface area and micropore volume (Table 4). The activation treatment enabled further development of the porous structure of BC by creating new internal pores and channels. The paired *t*-test results indicated that the effect of physical activation on the formaldehyde removal capacity was statistically significant (p = 0.001). A deeper study on the air purification performance of BC with and without activation is required to assess the environmental benefits of choosing non-activated or activated BC because of their pollutant removal capacity.

3.3 Formaldehyde removal in function of time and re-usability of the biocarbon

Figure 6 represents the evolution of formaldehyde concentrations inside the test chamber during 1 h of experimental time.

The decrease in formaldehyde concentrations was fast during the first 20 min of the experiment for AD and OS-derived BC. After approximately 20 min, the adsorption slowed, and the formaldehyde concentrations stabilized (Figure 5). Indeed, at the experiment's beginning, the BC structure pores were free and served as sites for the formaldehyde molecules. When most pores were occupied and the equilibrium time was reached, the adsorption process gradually decreased and stabilized, suggesting that the BC samples became saturated. The equilibrium time was slightly more delayed for samples prepared at temperatures above 500°C given that the formaldehyde capture mainly depended on pores filling. Similarly, Aziz et al. (2017) found that the adsorption capacity of zeolite-based adsorbents towards aromatic VOCs gradually decreased after reaching the respective equilibrium time (approximately 25 min).

Figure 7 represents the formaldehyde removal percentages of AD-BC800 after five cycles of thermal regeneration, which consists of using heat transfer forces to release the adsorbed formaldehyde molecules from the BC pores.

It was observed that the AD-BC800 sample maintained a comparable formaldehyde removal capacity up to the fourth cycle, indicating that it was possible to desorb formaldehyde molecules. After heating, BC's pores were freed and available for a new adsorption cycle. However, the removal capacity decreased by 13% after the fifth cycle, indicating that the re-usability of BC adsorbent tended to decline after several regeneration cycles. This result was attributed to the changes in structure and surface properties of the BC that likely occurred after repeated heating cycles. Prior research (Ahn et al., 2021) found that the formaldehyde adsorption capacity onto metal-BC decreased by about 50% and 65% after the first and second cycles of thermal regeneration at 80°C for 1 day, respectively. They explained that changes might have occurred in the pores structure and surface chemistry of the metal-BC, contributing to a partial loss in the adsorption performances. Moreover, Yang et al. (2018) investigated the adsorption-desorption cycles of toluene onto activated carbon samples with variable pore sizes. They reported that the pollutants' molecules accumulated in the activated carbon's narrow micropores, making it challenging to desorb at low regeneration temperatures. Hence, other methods should be pursued to free the BC pores and allow a long-lasting

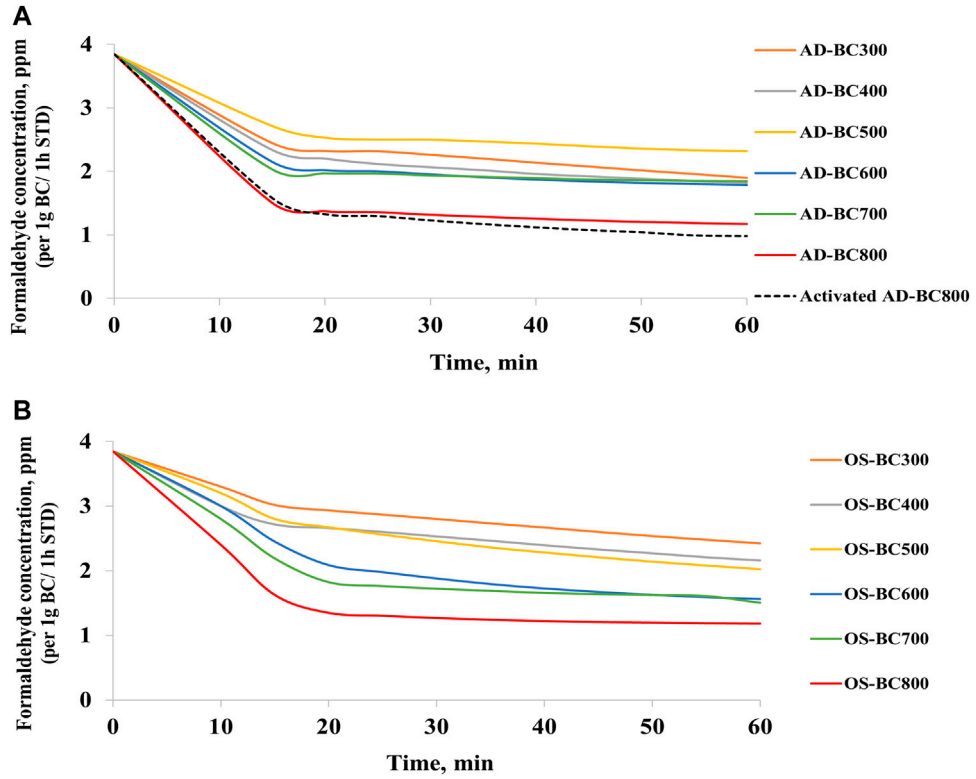

FIGURE 6
Variation of formaldehyde concentrations in the test chamber in the presence of **(A)** *Arundo donax* and **(B)** olive stone biocarbon.

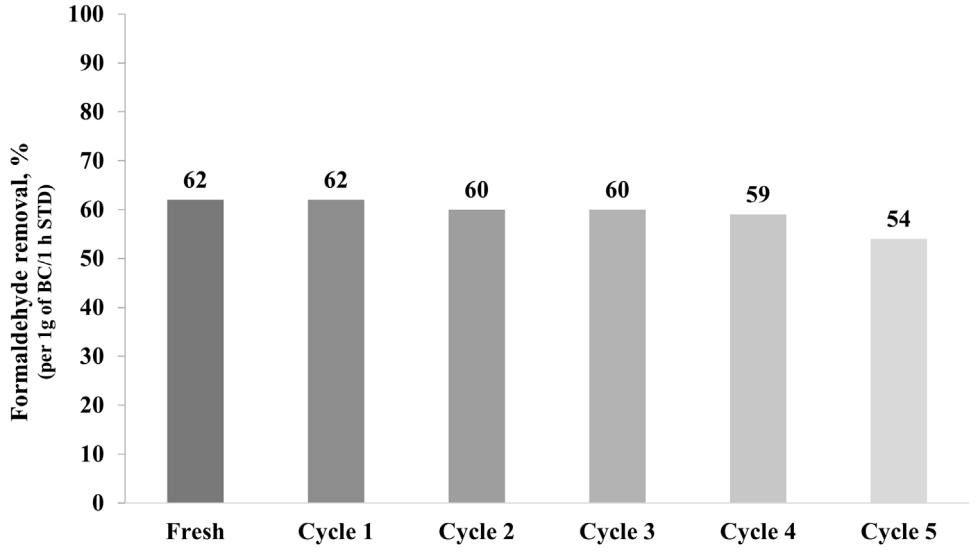

FIGURE 7
Formaldehyde removal capacity of AD-BC800 after five thermal regeneration cycles.

removal capacity. In this goal, follow-up research is conducted to dope BC particles with active photocatalysts and investigate the integrated adsorption-photocatalytic degradation potential.

The AD-BC800 sample was further tested using FTIR spectroscopy after the fifth adsorption and regeneration cycle to investigate eventual changes in the functional groups' composition. The spectra collected for

the fresh and re-used samples (Supplementary Figure S3) were similar. Hence, the second derivatives were also collected to enhance peak separation and reveal differences between the spectra. No obvious changes in the functional groups' composition were observed after the re-use and regeneration cycles except that the same peaks were slightly intensified. This result suggests that thermal regeneration effectively desorbs the formaldehyde from the spent material, especially since formaldehyde is characterized by high volatility. Prior research (Ahn et al., 2021) compared FTIR spectra of metallic biochar before and after interaction with formaldehyde. They observed new peaks at 2,900, 2,520, and 2,220 cm^{-1}, attributed to intermolecular hydrogen bonds of formate, carboxylic acid OH stretch, and alkyne stretching, respectively. However, they utilized metallic biochar, which facilitated the conversion of formaldehyde after adsorption and led to the appearance of intermediate molecules. Moreover, they collected the FTIR spectra directly after adsorption without performing a thermal regeneration step, which was not the case in the present study. Similarly (Chen et al., 2013), utilized Ag-containing catalysts for formaldehyde conversion, and they could identify several functional groups related to the occurrence of formaldehyde intermediates, such as formate species (HCOO) after interaction of the catalytic material with the formaldehyde gas. The investigation of variation in the adsorbent properties after several re-use cycles could be interesting to identify the cause of the decrease in formaldehyde removal efficiency after re-using, which will be considered in further research.

4 Conclusion

Biocarbon (BC) samples were prepared from *A. donax* (AD) and Olive stone (OS) at variable pyrolytic temperatures and used for capturing formaldehyde in batch experiments. The increase in pyrolysis temperature from 300°C to 800 °C increased the fixed carbon content of AD and OS-derived BC by 137% and 79%, respectively. The hydrophobicity and porosity of the BC increased with temperature. The FTIR showed that the surface functional groups occurred more in BC prepared at mild temperatures under 500 °C. The formaldehyde removal efficiencies ranged between 26% and 64%. The formaldehyde removal by BC prepared at temperatures under 500 °C was governed by a partitioning mechanism, favored by the presence of noncarbonized fraction that enabled the diffusion of formaldehyde molecules. Whereas for BC prepared at 500 °C or above, the formaldehyde removal was controlled by a physical adsorption mechanism assisted by pores filling. The occurrence of micropores in BC was a key parameter for optimal formaldehyde removal. The physical activation of AD-BC800 significantly increased the formaldehyde adsorption, which was attributed to the activated sample's enhanced microporosity. Thermally regenerated AD-BC800 exhibited comparable potential in removing formaldehyde for up to four re-use cycles. However, the formaldehyde removal percentage decreased by 13% in the fifth cycle, indicating that BC could partially lose its adsorptive function over long-term use. The saturation can limit BC's adsorptive potential after pores are filled with the adsorbate molecules. Therefore, for efficient use of BC in air remediation, it is necessary to find solutions to regenerate BC while preserving its performance effectively. Future research is warranted to develop BC particles that can degrade captured formaldehyde and investigate the adsorption degradation potential.

Data availability statement

The original contributions presented in the study are included in the article/Supplementary Material, further inquiries can be directed to the corresponding author.

Author contributions

MZ: Conceptualization, Investigation, Experimental, Formal analysis, Writing Original Draft. LM: Supervision, Review, Validation. DD: Supervision, Review, Editing. All authors contributed to the article and approved the submitted version.

Funding

This work was supported by the European Union's Horizon 2020 research and innovation program under H2020-WIDESPREAD-2018-2020-6 (grant agreement No 952395), the ForestValue Research Program and the Republic of Slovenia's Ministry of Education, Science and Sport (BarkBuild: grant agreement No C3330-21-252003), project BarkBuild is supported under the umbrella of ERA-NET cofund ForestValue 773324, and H2020 WIDESPREAD-2-Teaming (grant number 739574) and investment from the Republic of Slovenia and the European Regional Development Fund.

Conflict of interest

The authors declare that the research was conducted in the absence of any commercial or financial relationships that could be construed as a potential conflict of interest.

Publisher's note

Supplementary material

The Supplementary Material for this article can be found online at: https://www.frontiersin.org/articles/10.3389/fenvs.2023.1252926/full#supplementary-material

References

Abdul Manap, N. R., Shamsudin, R., Maghpor, M. N., Abdul Hamid, M. A., and Jalar, A. (2018). Adsorption isotherm and kinetic study of gas-solid system of formaldehyde on oil palm mesocarp bio-char: pyrolysis effect. *J. Environ. Chem. Eng.* 6, 970–983. doi:10.1016/j.jece.2017.12.067

Ahn, Y., Cho, D. W., Ahmad, W., Jo, J., Jurng, J., Kurade, M. B., et al. (2021). Efficient removal of formaldehyde using metal-biochar derived from acid mine drainage sludge and spent coffee waste. *J. Environ. Manage.* 298, 113468. doi:10.1016/j.jenvman.2021.113468

Angın, D. (2013). Effect of pyrolysis temperature and heating rate on biochar obtained from pyrolysis of safflower seed press cake. *Bioresour. Technol.* 128, 593–597. doi:10.1016/j.biortech.2012.10.150

ASTM (2015). *Standard Test Methods for Proximate Analysis of Coal and Coke by Macro Thermogravimetric Analysis*. West Conshohocken, PA: ASTM International.

Aziz, A., Kim, M., Kim, S., and Kim, K. S. (2017). Adsorption and kinetic studies of volatile organic compounds (VOCs) on seed assisted template free ZSM-5 zeolite in air. *J. Nanotechnol. Adv. Mater.* 9, 1–9. doi:10.18576/jnam/050101

Bachmann, J., Horton, R., van der Ploeg, R. R., and Woche, S. (2000). Modified sessile drop method for assessing initial soil–water contact angle of sandy soil. *Soil Sci. Soc. Am. J.* 64, 564–567. doi:10.2136/sssaj2000.642564x

Basu, P. (2013). "Chapter 5 - pyrolysis," in *Biomass gasification, pyrolysis and torrefaction*. Editor P. Basu (Boston: Academic Press), 147–176. doi:10.1016/B978-0-12-396488-5.00005-8

Boonamnuayvitaya, V., Sae-ung, S., and Tanthapanichakoon, W. (2005). Preparation of activated carbons from coffee residue for the adsorption of formaldehyde. *Sep. Purif. Technol.* 42, 159–168. doi:10.1016/j.seppur.2004.07.007

Carter, E. M., Katz, L. E., Speitel, G. E., and Ramirez, D. (2011). Gas-phase formaldehyde adsorption isotherm studies on activated carbon: correlations of adsorption capacity to surface functional group density. *Environ. Sci. Technol.* 45, 6498–6503. doi:10.1021/es104286d

Chen, B., Zhou, D., and Zhu, L. (2008). Transitional adsorption and partition of nonpolar and polar aromatic contaminants by biochars of pine needles with different pyrolytic temperatures. *Environ. Sci. Technol.* 42, 5137–5143. doi:10.1021/es8002684

Chen, D., Qu, Z., Sun, Y., Gao, K., and Wang, Y. (2013). Identification of reaction intermediates and mechanism responsible for highly active HCHO oxidation on Ag/MCM-41 catalysts. *Appl. Catal. B Environ.* 142–143, 838–848. doi:10.1016/j.apcatb.2013.06.025

Do, S. B., Lee, S. E., and Kim, T. O. (2022). Oxidative decomposition with PEG-MnO2 catalyst for removal of formaldehyde: chemical aspects on HCHO oxidation mechanism. *Appl. Surf. Sci.* 598, 153773. doi:10.1016/j.apsusc.2022.153773

Egbosiuba, T. C., Abdulkareem, A. S., Kovo, A. S., Afolabi, E. A., Tijani, J. O., Auta, M., et al. (2020). Ultrasonic enhanced adsorption of methylene blue onto the optimized surface area of activated carbon: adsorption isotherm, kinetics and thermodynamics. *Chem. Eng. Res. Des.* 153, 315–336. doi:10.1016/j.cherd.2019.10.016

Egbosiuba, T. C. (2022). Biochar and bio-oil fuel properties from nickel nanoparticles assisted pyrolysis of cassava peel. *Heliyon* 8, e10114. doi:10.1016/j.heliyon.2022.e10114

Ferreiro-Cabello, J., Fraile-Garcia, E., Pernia-Espinoza, A., and Martinez-de-Pison, F. J. (2022). Strength performance of different mortars doped using olive stones as lightweight aggregate. *Buildings* 12, 1668. doi:10.3390/buildings12101668

Guo, Z., Huang, J., Xue, Z., and Wang, X. (2016). Electrospun graphene oxide/carbon composite nanofibers with well-developed mesoporous structure and their adsorption performance for benzene and butanone. *Chem. Eng. J.* 306, 99–106. doi:10.1016/j.cej.2016.07.048

IARC (2006). *IARC monographs on the evaluation of carcinogenic risks to humans*. 1st ed. Lyon, France: IARC. Available at: https://publications.iarc.fr/Book-And-Report-Series/Iarc-Monographs-On-The-Identification-Of-Carcinogenic-Hazards-To-Humans/Formaldehyde-2-Butoxyethanol-And-1–Em-Tert-Em–Butoxypropan-2-ol-2006 (Accessed December 17, 2022).

Keiluweit, M., Nico, P. S., Johnson, M. G., and Kleber, M. (2010). Dynamic molecular structure of plant biomass-derived black carbon (biochar). *Environ. Sci. Technol.* 44, 1247–1253. doi:10.1021/es9031419

Law, K. Y. (2014). Definitions for hydrophilicity, hydrophobicity, and superhydrophobicity: getting the basics right. *J. Phys. Chem. Lett.* 5, 686–688. doi:10.1021/jz402762h

Lee, J. Y., Park, S. H., Jeon, J. K., Yoo, K. S., Kim, S. S., and Park, Y. K. (2011). The removal of low concentration formaldehyde over sewage sludge char treated using various methods. *Korean J. Chem. Eng.* 28, 1556–1560. doi:10.1007/s11814-011-0007-7

Leng, L., and Huang, H. (2018). An overview of the effect of pyrolysis process parameters on biochar stability. *Bioresour. Technol.* 270, 627–642. doi:10.1016/j.biortech.2018.09.030

Ling, Y., Wang, Y., Duan, J., Xie, X., Liu, Y., Peng, Y., et al. (2019). Long-term aerosol size distributions and the potential role of volatile organic compounds (VOCs) in new particle formation events in Shanghai. *Atmos. Environ.* 202, 345–356. doi:10.1016/j.atmosenv.2019.01.018

Liu, L., Liu, J., Zeng, Y., Tan, S. J., Do, D. D., and Nicholson, D. (2019). Formaldehyde adsorption in carbon nanopores – new insights from molecular simulation. *Chem. Eng. J.* 370, 866–874. doi:10.1016/j.cej.2019.03.262

Liu, W., Li, Z., Zhang, S., Jian, W., and Ma, D. (2021). Adsorption performance of multi-walled carbon nanotube-SiO2 adsorbent for toluene. *J. Fuel Chem. Technol.* 49, 861–872. doi:10.1016/S1872-5813(21)60090-7

Lu, S., and Zong, Y. (2018). Pore structure and environmental serves of biochars derived from different feedstocks and pyrolysis conditions. *Environ. Sci. Pollut. Res.* 25, 30401–30409. doi:10.1007/s11356-018-3018-7

Mao, J., Zhang, K., and Chen, B. (2019). Linking hydrophobicity of biochar to the water repellency and water holding capacity of biochar-amended soil. *Environ. Pollut.* 253, 779–789. doi:10.1016/j.envpol.2019.07.051

Marrot, L., Candelier, K., Valette, J., Lanvin, C., Horvat, B., Legan, L., et al. (2021). Valorization of hemp stalk waste through thermochemical conversion for energy and electrical applications. *Waste Biomass Valorization* 13, 2267–2285. doi:10.1007/s12649-021-01640-6

Marrot, L., Zouari, M., Schwarzkopf, M., and DeVallance, D. B. (2023). Sustainable biocarbon/tung oil coatings with hydrophobic and UV-shielding properties for outdoor wood substrates. *Prog. Org. Coat.* 177, 107428. doi:10.1016/j.porgcoat.2023.107428

Meng, F., Song, M., Wei, Y., and Wang, Y. (2019). The contribution of oxygen-containing functional groups to the gas-phase adsorption of volatile organic compounds with different polarities onto lignin-derived activated carbon fibers. *Environ. Sci. Pollut. Res.* 26, 7195–7204. doi:10.1007/s11356-019-04190-6

Meyer, B., and Boehme, C. (1997). Formaldehyde emission from solid wood. *For. Prod. J.* 47, 45–48.

Naito, M., Hayakawa, O., Nakahira, K., Mori, H., and Tsubaki, J. (1998). Effect of particle shape on the particle size distribution measured with commercial equipment. *Powder Technol.* 100, 52–60. doi:10.1016/S0032-5910(98)00052-7

Nandiyanto, A., Fadhlulloh, M., Rahman, T., and Mudzakir, A. (2016). Synthesis of carbon nanoparticles from commercially available liquified petroleum gas. *IOP Conf. Ser. Mater. Sci. Eng.* 128, 012042. doi:10.1088/1757-899X/128/1/012042

Rodríguez, G., Lama, A., Rodríguez, R., Jiménez, A., Guillén, R., and Fernández-Bolaños, J. (2008). Olive stone an attractive source of bioactive and valuable compounds. *Bioresour. Technol.* 99, 5261–5269. doi:10.1016/j.biortech.2007.11.027

Ryu, Y. K., Lee, H. J., Yoo, H. K., and Lee, C. H. (2002). Adsorption equilibria of toluene and gasoline vapors on activated carbon. *J. Chem. Eng. Data* 47, 1222–1225. doi:10.1021/je020044i

Sachdeva, S., Kumar, R., Sahoo, P. K., and Nadda, A. K. (2023). Recent advances in biochar amendments for immobilization of heavy metals in an agricultural ecosystem: a systematic review. *Environ. Pollut.* 319, 120937. doi:10.1016/j.envpol.2022.120937

Sahoo, K., Kumar, A., and Chakraborty, J. (2020). A comparative study on valuable products: bio-oil, biochar, non-condensable gases from pyrolysis of agricultural residues. *J. Mater. Cycles Waste Manag.* 39, 186–204. doi:10.1007/s10163-020-01114-2

Salthammer, T., Mentese, S., and Marutzky, R. (2010). Formaldehyde in the indoor environment. *Chem. Rev.* 110, 2536–2572. doi:10.1021/cr800399g

Stylianou, M., Christou, A., Michael, C., Agapiou, A., Papanastasiou, P., and Fatta-Kassinos, D. (2021). Adsorption and removal of seven antibiotic compounds present in water with the use of biochar derived from the pyrolysis of organic waste feedstocks. *J. Environ. Chem. Eng.* 9, 105868. doi:10.1016/j.jece.2021.105868

Suárez, L., Castellano, J., Romero, F., Marrero, M. D., Benítez, A. N., and Ortega, Z. (2021). Environmental hazards of giant reed (Arundo donax L.) in the macaronesia region and its characterisation as a potential source for the production of natural fibre composites. *Polymers* 13, 2101. doi:10.3390/polym13132101

Thommes, M., Kaneko, K., Neimark, A. V., Olivier, J. P., Rodriguez-Reinoso, F., Rouquerol, J., et al. (2015). Physisorption of gases, with special reference to the evaluation of surface area and pore size distribution (IUPAC Technical Report). *Pure Appl. Chem.* 87, 1051–1069. doi:10.1515/pac-2014-1117

Uchimiya, M., Wartelle, L. H., Klasson, K. T., Fortier, C. A., and Lima, I. M. (2011). Influence of pyrolysis temperature on biochar property and function as a heavy metal sorbent in soil. *J. Agric. Food Chem.* 59, 2501–2510. doi:10.1021/jf104206c

US National Research Council (1980). *Formaldehyde - an assessment of its health effects*. 1st ed. Washington DC: National Academies Press US. Available at: https://www.ncbi.nlm.nih.gov/books/NBK217652/(Accessed December 17, 2022).

Van Krevelen, W. D. (1993). *Coal: typology - physics - chemistry - constitution*. 1st ed. Amsterdam, Netherlands: Elsevier Science Publishers. Available at: https://www.osti.gov/etdeweb/biblio/5331158 (Accessed December 18, 2022).

Vikrant, K., Kim, K. H., Peng, W., Ge, S., and Sik Ok, Y. (2020). Adsorption performance of standard biochar materials against volatile organic compounds in air: a case study using benzene and methyl ethyl ketone. *Chem. Eng. J.* 387, 123943. doi:10.1016/j.cej.2019.123943

WHO (2022). Household air pollution. Available at: https://www.who.int/news-room/fact-sheets/detail/household-air-pollution-and-health (Accessed December 16, 2022).

WHO (1989). Indoor air quality: organic pollutants. *Environ. Technol. Lett.* 10, 855–858. doi:10.1080/09593338909384805

Yang, H., Yan, R., Chen, H., Lee, D. H., and Zheng, C. (2007). Characteristics of hemicellulose, cellulose and lignin pyrolysis. *Fuel* 86, 1781–1788. doi:10.1016/j.fuel.2006.12.013

Yang, S., Zhu, Z., Wei, F., and Yang, X. (2017). Enhancement of formaldehyde removal by activated carbon fiber via *in situ* growth of carbon nanotubes. *Build. Environ.* 126, 27–33. doi:10.1016/j.buildenv.2017.09.025

Yang, X., Yi, H., Tang, X., Zhao, S., Yang, Z., Ma, Y., et al. (2018). Behaviors and kinetics of toluene adsorption-desorption on activated carbons with varying pore structure. *J. Environ. Sci.* 67, 104–114. doi:10.1016/j.jes.2017.06.032

Yu, K. L., Lee, X. J., Ong, H. C., Chen, W. H., Chang, J. S., Lin, C. S., et al. (2021). Adsorptive removal of cationic methylene blue and anionic Congo red dyes using wet-torrefied microalgal biochar: equilibrium, kinetic and mechanism modeling. *Environ. Pollut.* 272, 115986. doi:10.1016/j.envpol.2020.115986

Zhang, X., Gao, B., Zheng, Y., Hu, X., Creamer, A. E., Annable, M. D., et al. (2017). Biochar for volatile organic compound (VOC) removal: sorption performance and governing mechanisms. *Bioresour. Technol.* 245, 606–614. doi:10.1016/j.biortech.2017.09.025

Zouari, M., Marrot, L., and DeVallance, D. B. (2023). Effect of demineralization and ball milling treatments on the properties of Arundo donax and olive stone-derived biochar. *Int. J. Environ. Sci. Technol.* doi:10.1007/s13762-023-04968-9